Supporting Information for "Mapping the seismicity of Mars with InSight"

S. Ceylan[1], D. Giardini[1], J. F. Clinton[2], D. Kim[1], A. Khan[1,3], S. C. Stähler[1,4], G. Zenhäusern[1], P. Lognonné[5], and W. B. Banerdt[6]

[1]Institute of Geophysics, ETH Zurich, Zurich, Switzerland
[2]Swiss Seismological Service, ETH Zurich, Zurich, Switzerland
[3]Institute of Geochemistry and Petrology, ETH Zurich, Zurich, Switzerland
[4]Physik-Institut, University of Zurich, Zurich, Switzerland
[5]Université Paris Cité, Institut de physique du globe de Paris, CNRS, Paris, France
[6]Jet Propulsion Laboratory, California Institute of Technology, Pasadena, CA, USA

Contents of this file

1. Figures S1 to S12
2. Tables S1 and S2

Introduction

In Table S1, we provide a breakdown of the V14 seismicity catalog from InSight (InSight Marsquake Service, 2023). Table S2 contains a list of re-evaluated events with a summary of modification proposed here. Figure S1 compares magnitude and distance distribution in V14 catalog and this study. The envelope computation steps and resulting cost matrix from similarity analysis are shown in Figure S2 and Figure S3, respectively. Figures S4–S6 demonstrate test cases for the backazimuth determination using grid search approach. Figure S7 show similarity analysis for 3 event classes. Figure S8 provides a summary of S1153a and S1415a. An additional comparison for S0235b and S0173a is provided in Figure S9. Interpretation and relocation of event classes are in Figures S10–S12.

Table S1: Breakdown of the MQS catalog V14 (InSight Marsquake Service, 2023). Events are classified into low-frequency (LF) and high-frequency (HF) families. The LF family is further classified into two types as LF and broadband (BB) events. The HF family consists of the 2.4 Hz, HF, very high-frequency (VF) sub-classes. Each event is cataloged with a quality identifier (QA being the highest quality and QD the most speculative) depending on the signal-to-noise ratio and reliability of phase picks. More information on the event classification is available in Clinton et al. (2021) and Ceylan et al. (2022). This study focuses on the LF family events only.

Event type	Total	QA	QB	QC	QD
Low-frequency family					
LF	59	6	12	20	21
BB	39	8	10	15	6
High-frequency family					
2.4Hz	989	–	50	353	586
HF	162	–	74	79	9
VF	74	–	29	34	11
Total	1319	14	175	500	630

Table S2: Breakdown of re-evaluated events and summary of the analysis done in this study.

Event name	Distance (°) in V14	Backazimuth (°) in V14	Distance (°) this study	Backazimuth (°) this study
Cerberus Fossae events: 18 events. Re-located at the center of the Cerberus Fossae system, using the original distances as reported in V14.				
S0105a	32.5±8.2	112±19	–	85±5
S0173a	30±1.4	88±11	–	85±5
S0235b	28.5±1.5	77±11	–	85±5
S0407a	29.3±2	90±62	–	85±5
S0474a	29.1±18	97±13	–	85±5
S0484b	31.8±5.9	100±20	–	85±5
S0784a	34.4±3.5	115±22	–	85±5
S0802a	30±3.5	82±15	–	85±5
S0809a	29.8±2	91±9	–	85±5
S0820a	30.2±2.4	106±17	–	85±5
S0864a	28.7±3.5	90±22	–	85±5
S0916d	29.3±5.9	97±36.5	–	85±5
S1015f	27.5±2	89±25	–	85±5
S1022a	30.7±2	63±5	–	85±5
S1048d	30.2±1.3	97±17	–	85±5
S1133c	30.2±1.3	91±14	–	85±5
Events with weak or no S-wave: 4 events. New distances assigned to S0899d and S1097a. New backazimuth assigned to S1012d and S1197a, and combined with the previously reported distances, the events are now located.				
S0899d	46.7±10*	22±30	32±10	–
S1197a	32.0±1.5	–	–	65±40
S1097a	46.2±10*	318±20	32±10	–
S1012d	38.2±3.3	–	–	60±35
Events similar to S1094b[I]: 2 events. No modifications made.				
S0185a	59.8±20	–	–	–
S0234c	–	–	60±20	–
S1153a and S1415a: 2 events Backazimuth determined for S1153a. Both events are located SW of Olympus Mons.				
S1153a	84.8±10	–	–	85±30
S1415a	88.2±9.6	–	–	85±30
Distant cluster: 5 events. Distance assigned between 130–140° Located in the western Valles Marineris region using the S0976a backazimuth (101±25).				
S0154a	–	–	130–140	101±25
S0395a	–	–	130–140	101±25
S0345a	–	–	130–140	101±25
S0226b	–	–	130–140	101±25
S0133a	–	–	130–140	101±25

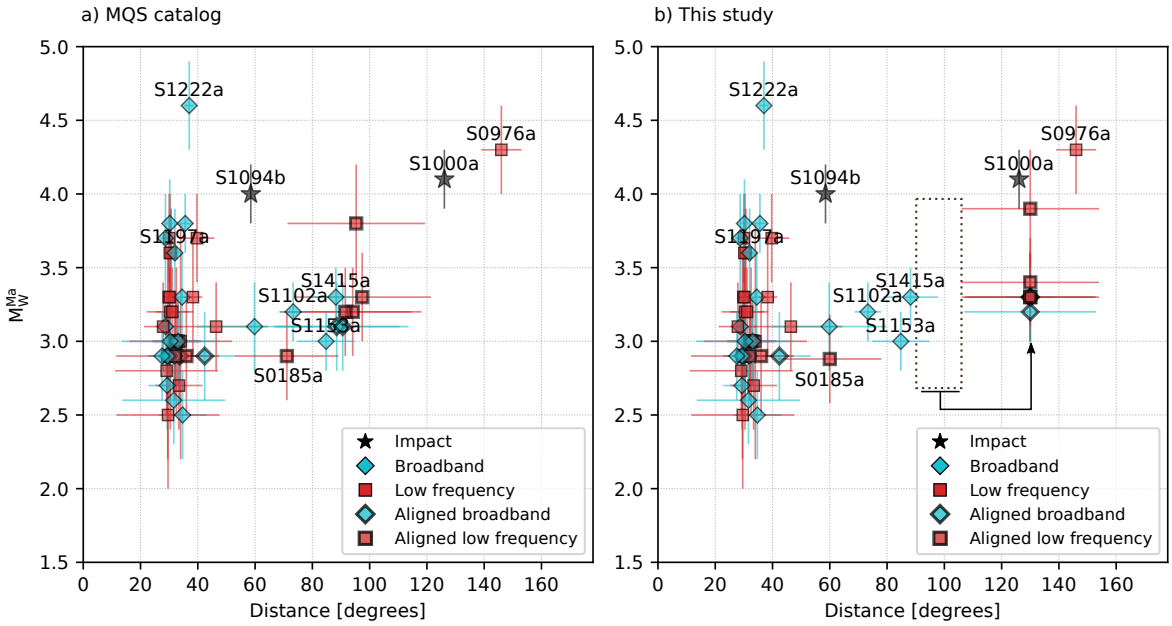

Figure S1: Distance vs Mars-calibrated moment magnitude (M_W^{Ma}; Böse et al., 2018) distribution of the events (a) in the V14 MQS catalog and (b) after our interpretations in this study. The stars show the impacts. The distance values for the events with thicker symbol edges come from visual alignments.

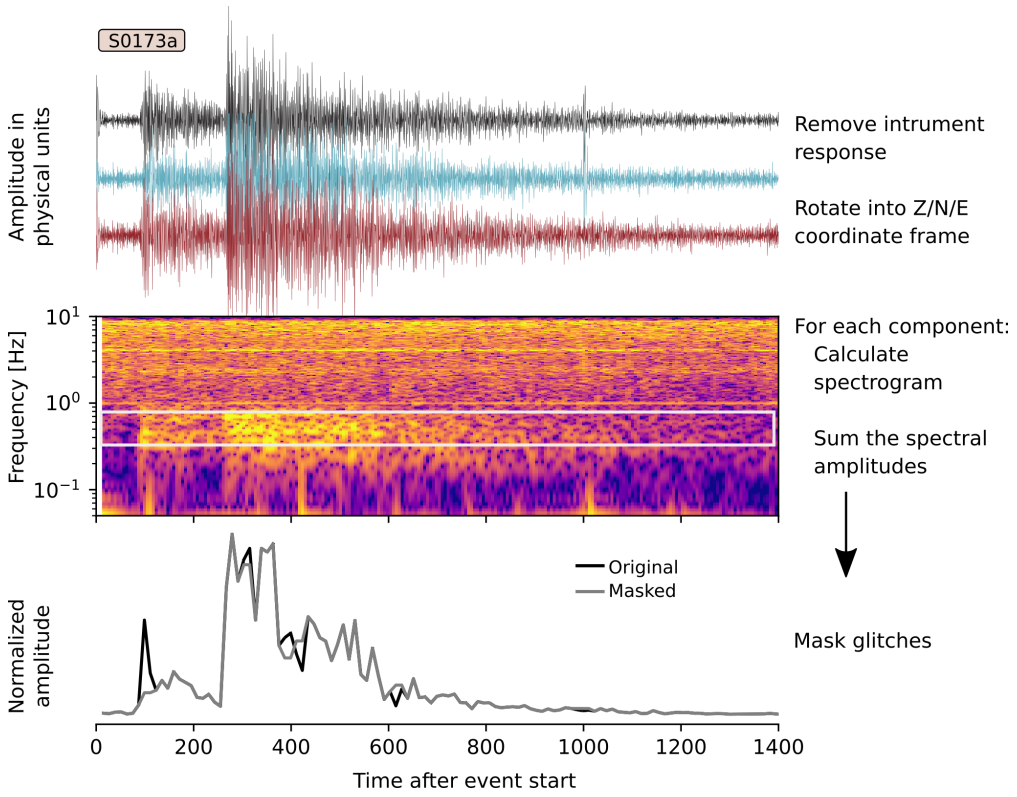

Figure S2: A sketch summarizing the envelope computation process using an example from S0173a (LF, quality A). The white rectangle in the middle panel represents the part of the spectrogram is used to create the envelope. Envelopes are computed by summing the spectral amplitudes along the frequency axis, then MQS-picked glitches are masked (bottom panel). These masked envelopes are used as input for the Dynamic Time Warping (DTW) (Sakoe and Chiba, 1978).

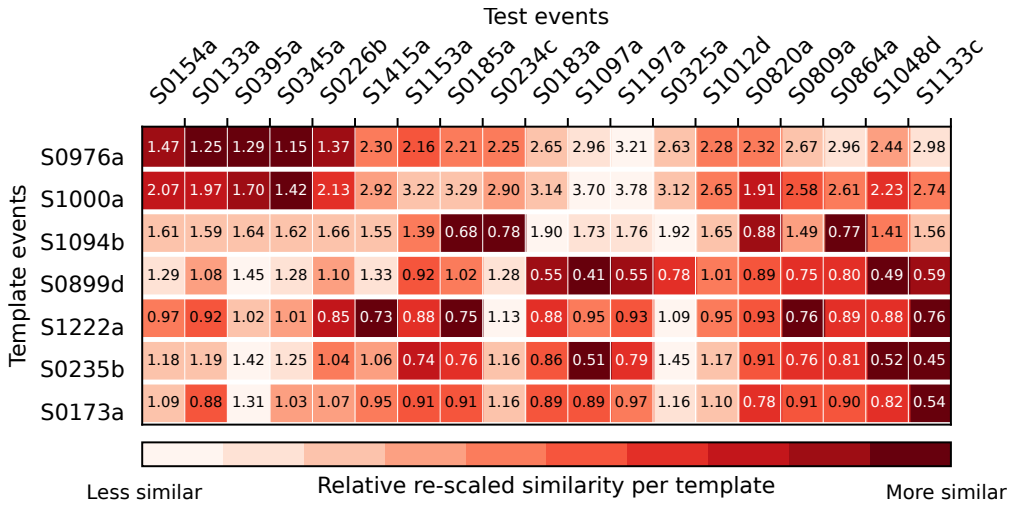

Figure S3: The cost matrix resulting from cross-similarity checks between the templates and test events discussed in this study. The DTW distances for event pairs are indicated in each cell. The colorbar shows the re-scaled relative similarity values per template event (rows) where lighter colors indicate less similarity.

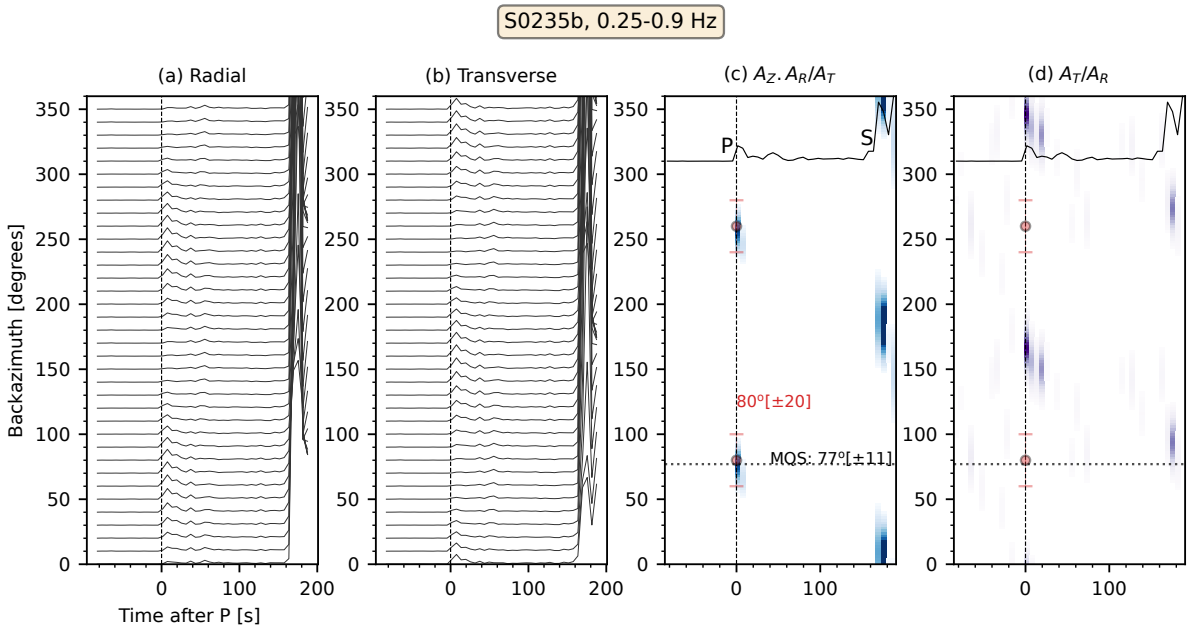

Figure S4: Test case for backazimuth estimation using our grid search approach for S0235b. The envelopes are computed for frequencies between 0.25 and 0.9 Hz. (a) and (b) show the rotated envelopes after normalization. (c) and (d) denote combined vertical (Z) and radial (R) to transverse (T) and T/R ratio, respectively. The estimated values from the grid search method and MQS are indicated. The orange dots with error bars show our preferred backzimuth pick, computed using envelope amplitudes before normalization. The envelopes for the vertical component are plotted at the top of (c) and (d) for reference.

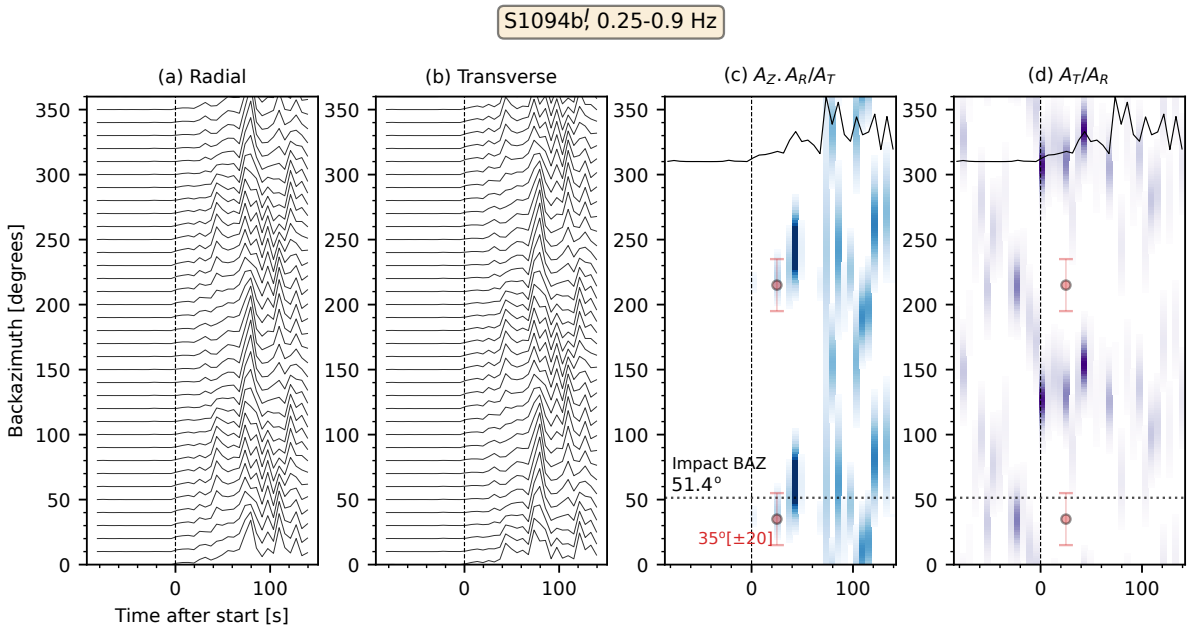

Figure S5: Backazimuth estimation for S1094b^I. The true location is 58.5° away from InSight with a backazimuth of 51.4° (Posiolova et al., 2022). Other details follow Figure **S4** caption.

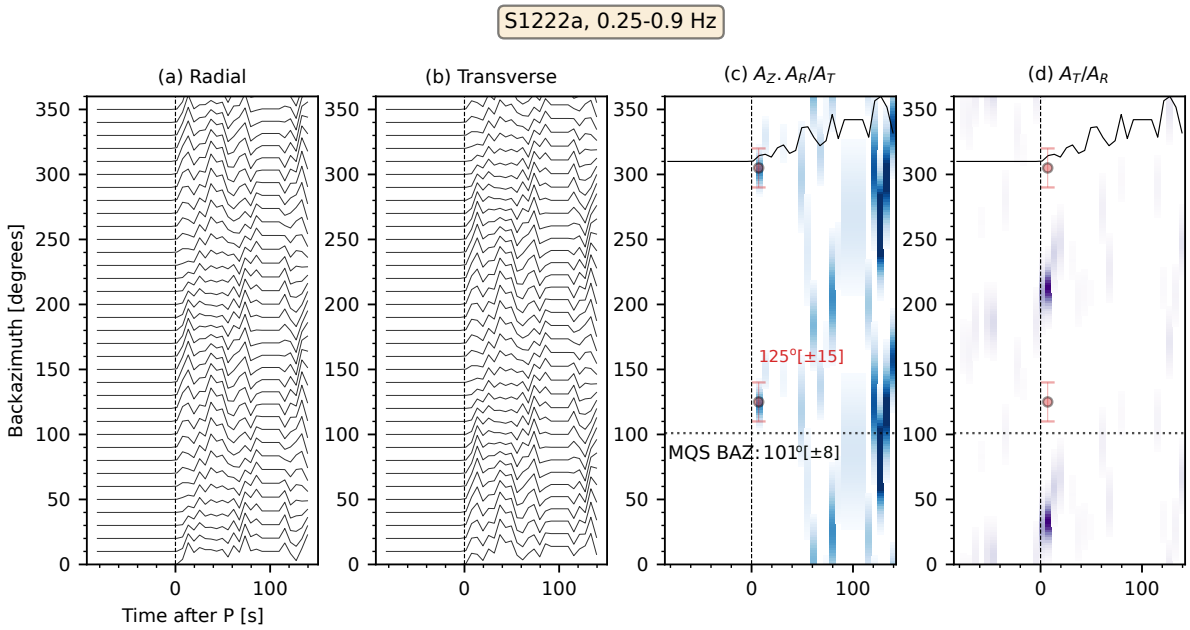

Figure S6: Test case for backazimuth estimation using S1222a. For this event, MQS computed a backazimuth of 101±8°. The figure caption follows Figure **S4**.

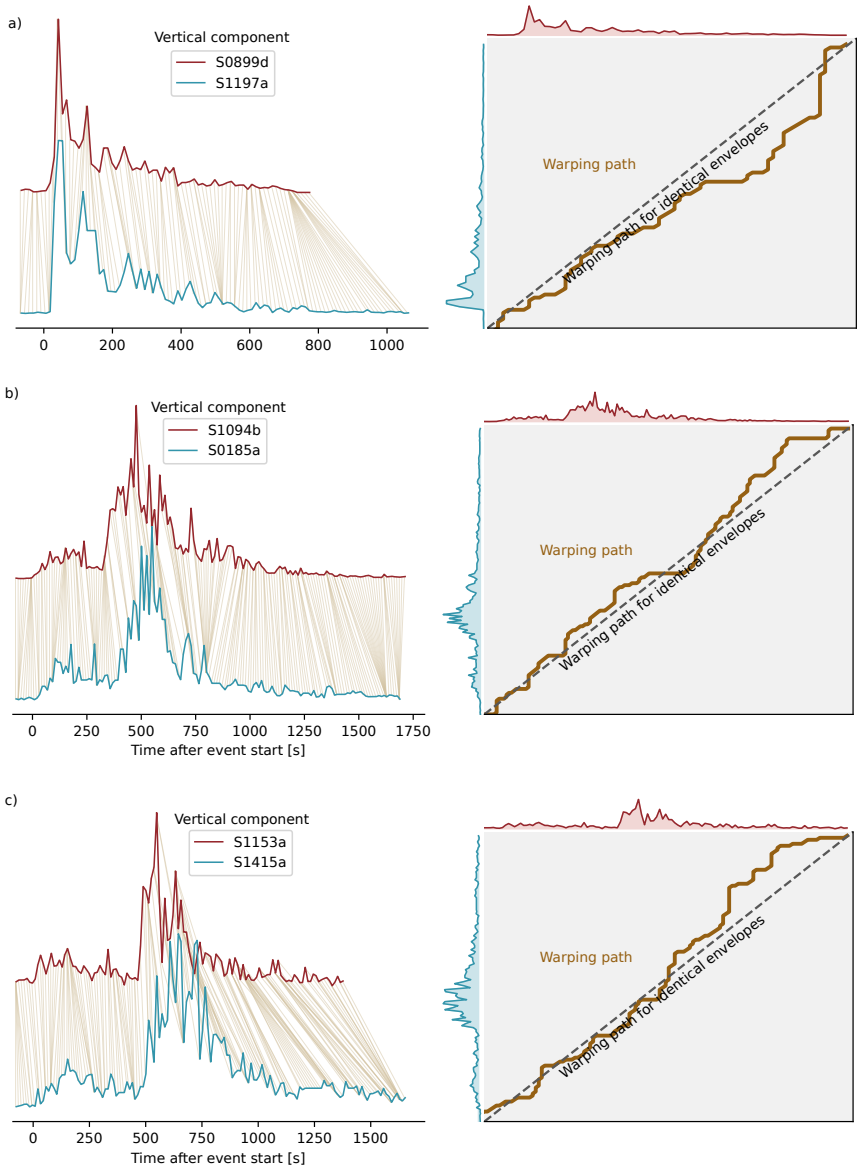

Figure S7: Warping path examples for 3 event classes. (a) S0899d and S1197a for weak-or-no S class, (b) S1094b^I and S0185a for events similar to the impact, and (c) S1153a and S1415a event pair.

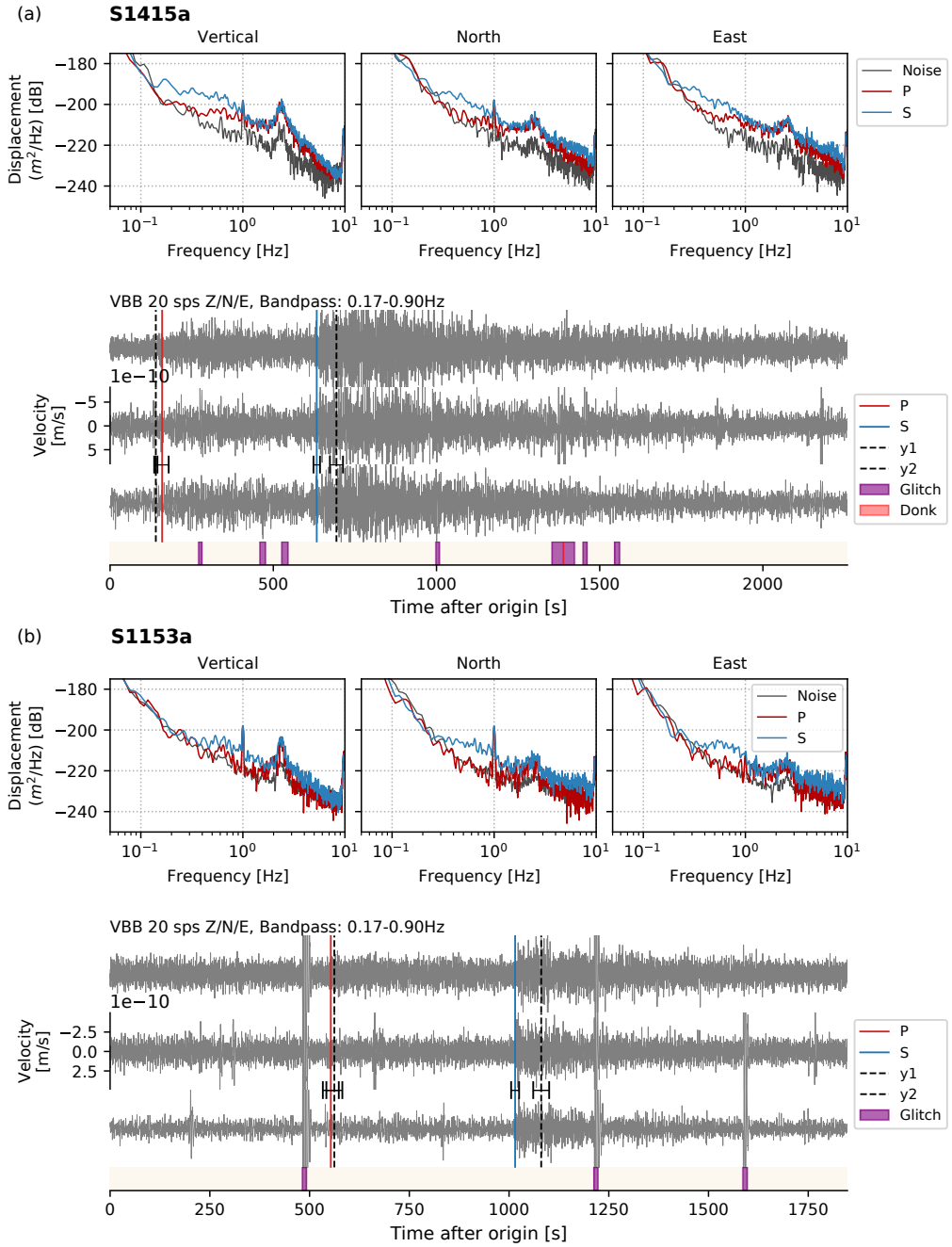

Figure S8: Event summary for S1415a (a) and S1153a (b), both broadband, quality B. Noise and signal windows in the displacement spectra are hand-picked by MQS. The seismic phases from MQS are shown with vertical lines with their picking uncertainties. The y1 and y2 phases (dashed lines) were picked on the high-frequency energy around 2.4 Hz.

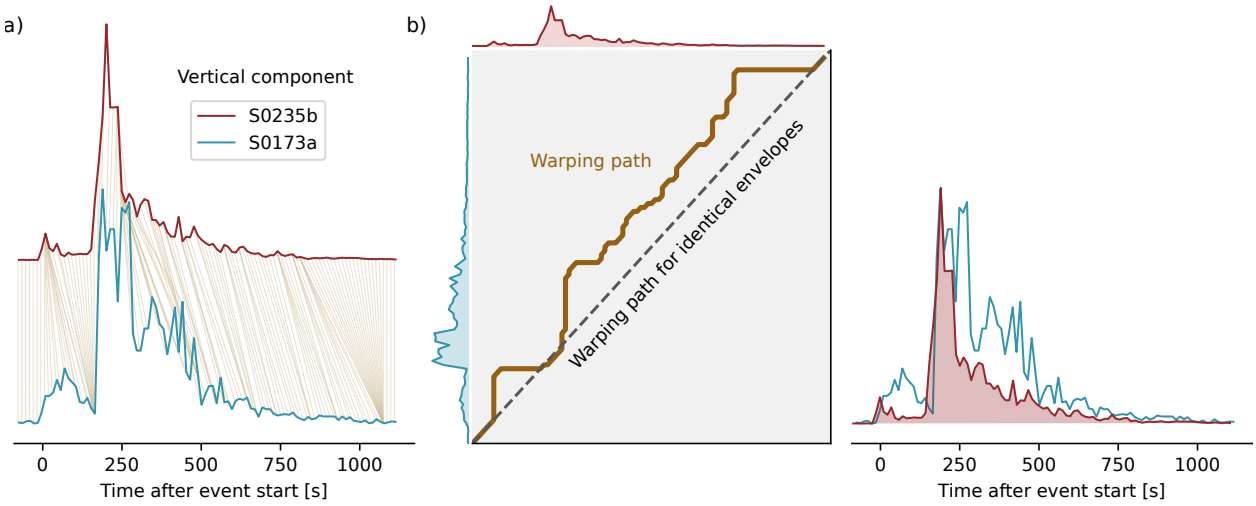

Figure S9: Comparison of S0235b and S0173a. (a) Point-wise warping match. (b) The warping path and envelopes in (a) overlapped. Note that the excess energy in the P- and S-coda makes similarity analysis harder although these two events originate from Cerberus Fossae and belong to the same class.

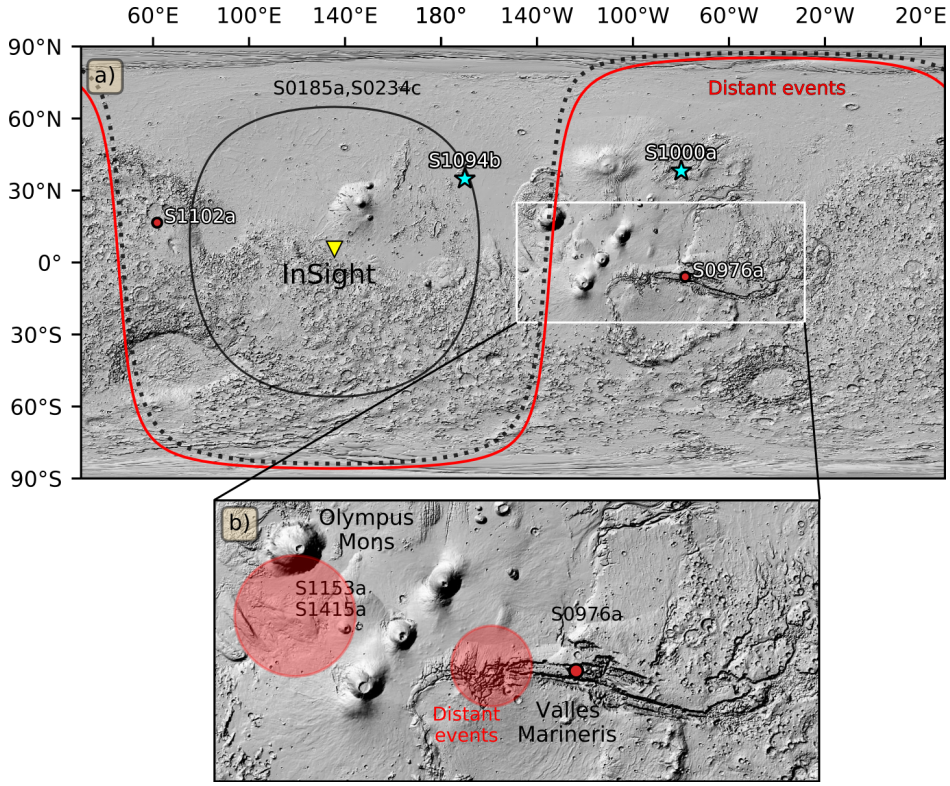

Figure S10: Interpretation of the events >60°. In (a), we show the most recent understanding from MQS. The panel (b) shows our interpretation for these events, zooming around the Valles Marineris region. The locations of the two known impacts are marked as cyan stars. The distant events (red curve in (a)) are located at the western Valles Marineris region (labelled as distant events in (b)). MQS computed distances of S1153a and S1415a, but no backazimuth was provided. We propose a backazimuth of 85±35° for S1153a (dotted black line in (a)), and due to their similarity, locate the events in western Tharsis region at Olympus Mons.

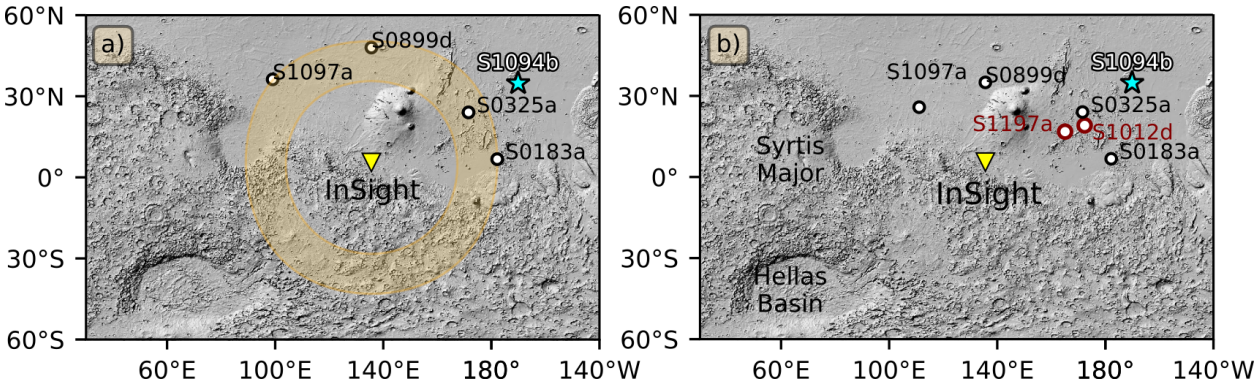

Figure S11: Interpretation of the events with no or weak S-wave energy. The template event is S0899d. (a) The current state in the MQS catalog (InSight Marsquake Service, 2023). The wheat-colored ring denotes the distance range (∼32-46°) which this class of events span. The S1094b^I is shown with cyan star at 58.5° as a reference to distance ranges. (b) Our interpretation of event locations. We refrain the locations provided by MQS; in addition, we locate two more events (S1012d and S1197a) after our backazimuth analysis. We identify S-phases for S0899d and S1097a, and locate the events at 31–32° range.

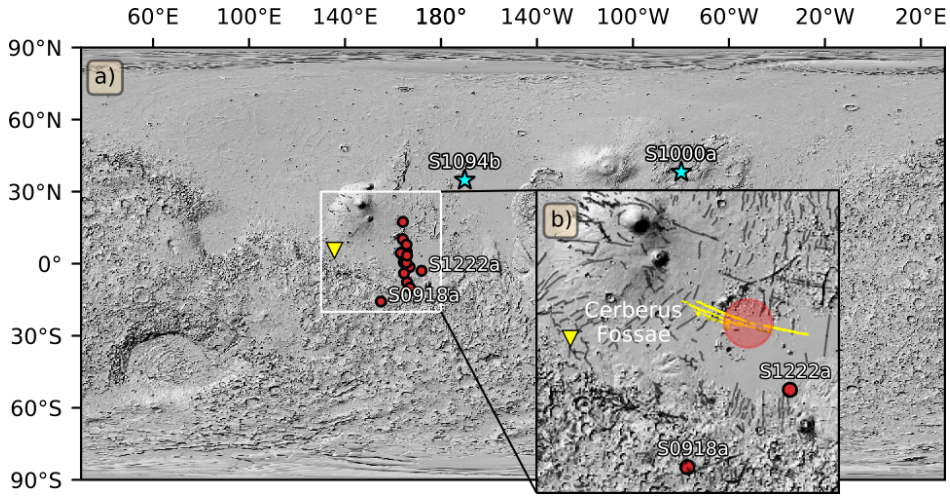

Figure S12: Interpretation of the events located in the Cerberus Fossae region. (a) Current MQS locations (red circles), and (b) our explanation of the seismicity. The faults in (b) are from Knapmeyer et al. (2006) and Perrin et al. (2022). The MQS event locations follow a North-South trend; however, the Cerberus fault system (yellow lines is (b) in NW-SE direction. Therefore, we project all events to the center. S1222a and S0918a are excluded due to their outlier locations.

References

Böse, M., D. Giardini, S. Stähler, S. Ceylan, J. F. Clinton, et al. (2018). "Magnitude Scales for Marsquakes". In: *Bull. Seismol. Soc. Am.* 108.5A, pp. 2764–2777. ISSN: 0037-1106. DOI: https://doi.org/10.1785/0120180037.

Ceylan, S., J. F. Clinton, D. Giardini, S. C. Stähler, A. Horleston, et al. (2022). "The marsquake catalogue from InSight, sols 0–1011". In: *Phys. Earth Planet. Inter.*, p. 106943. DOI: https://doi.org/10.1016/j.pepi.2022.106943.

Clinton, J., S. Ceylan, M. van Driel, D. Giardini, S. Stähler, et al. (2021). "The Marsquake catalogue from InSight, sols 0–478". In: *Phys. Earth Planet. Inter.* 310, p. 106595. ISSN: 0031-9201. DOI: https://doi.org/10.1016/j.pepi.2020.106595.

InSight Marsquake Service (2023). *Mars Seismic Catalogue, InSight Mission; V14 2023-04-01*. en. DOI: 10.12686/a21. URL: https://www.insight.ethz.ch/seismicity/catalog/v14.

Knapmeyer, M., J. Oberst, E. Hauber, M. Wählisch, C. Deuchler, and R. Wagner (2006). "Working models for spatial distribution and level of Mars' seismicity". In: *Journal of Geophysical Research: Planets* 111.E11, E11006. DOI: https://doi.org/10.1029/2006JE002708.

Perrin, C., A. Jacob, A. Lucas, R. Myhill, E. Hauber, et al. (2022). "Geometry and segmentation of Cerberus Fossae, Mars: Implications for Marsquake properties". In: *Journal of Geophysical Research: Planets* 127.1, e2021JE007118. DOI: https://doi.org/10.1029/2021JE007118.

Posiolova, L. V., P. Lognonné, W. B. Banerdt, J. Clinton, G. S. Collins, et al. (2022). "Largest recent impact craters on Mars: Orbital imaging and surface seismic co-investigation". In: *Science* 378.6618, pp. 412–417. DOI: 10.1126/science.abq7704.

Sakoe, H. and S. Chiba (1978). "Dynamic programming algorithm optimization for spoken word recognition". In: *IEEE Trans. Acoust.* 26.1, pp. 43–49. DOI: 10.1109/TASSP.1978.1163055.